THE JOURNAL OF PHYSICAL CHEMISTRY C
A JOURNAL OF THE AMERICAN CHEMICAL SOCIETY

pubs.acs.org/JPCC

Article

Atmospheric-Pressure Plasma-Enhanced Spatial ALD of SiO_2 Studied by Gas-Phase Infrared and Optical Emission Spectroscopy

M. A. Mione, V. Vandalon, A. Mameli, W. M. M. Kessels,* and F. Roozeboom

Cite This: *J. Phys. Chem. C* 2021, 125, 24945−24957

Read Online

ACCESS | Metrics & More | Article Recommendations | Supporting Information

ABSTRACT: An atmospheric-pressure plasma-enhanced spatial atomic layer deposition (PE-s-ALD) process for SiO_2 using bisdiethylaminosilane (BDEAS, $SiH_2[NEt_2]_2$) and O_2 plasma is reported along with an investigation of its underlying growth mechanism. Within the temperature range of 100−250 °C, the process demonstrates self-limiting growth with a growth per cycle (GPC) between 0.12 and 0.14 nm and SiO_2 films exhibiting material properties *on par* with those reported for low-pressure PEALD. Gas-phase infrared spectroscopy on the reactant exhaust gases and optical emission spectroscopy (OES) on the plasma region are used to identify the species that are involved in the ALD process. Based on the identified species, we propose a reaction mechanism where BDEAS molecules adsorb on −OH surface sites through the exchange of one of the amine ligands upon desorption of diethylamine (DEA). The remaining amine ligand is removed through combustion reactions activated by the O_2 plasma species leading to the release of H_2O, CO_2, and CO in addition to products such as N_2O, NO_2, and CH-containing species. These volatile species can undergo further gas-phase reactions in the plasma as indicated by the observation of OH*, CN*, and NH* excited fragments in OES. Furthermore, the infrared analysis of the precursor exhaust gas indicated the release of CO_2 during precursor adsorption. Moreover, this analysis has allowed the quantification of the precursor depletion yielding values between 10 and 50% depending on the processing parameters. Besides providing insights into the chemistry of atmospheric-pressure PE-s-ALD of SiO_2, our results demonstrate that infrared spectroscopy performed on exhaust gases is a valuable approach to quantify relevant process parameters, which can ultimately help evaluate and improve process performance.

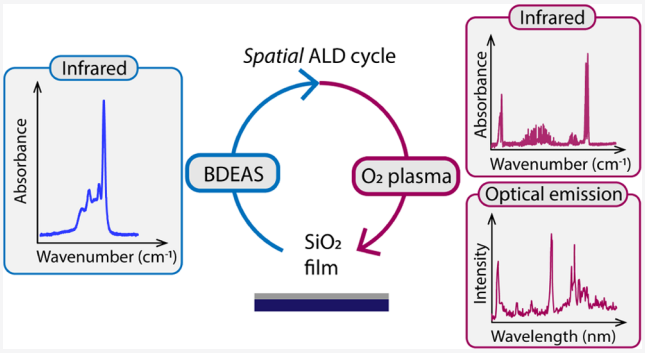

1. INTRODUCTION

The preparation of ultrathin, high-quality silicon oxide (SiO_2) films is essential for the fabrication of a multitude of devices in the fields of photovoltaics, microelectronics, displays, solar cell, photonics, etc.[1−3] SiO_2 films are employed as dielectric materials, surface passivation and encapsulation layers, optical coatings, and cladding materials.[4−6] Furthermore, SiO_2 films are used in the fabrication of nanoelectronic devices as dielectric or as sacrificial layers in self-aligned multiple patterning (SAxP) processes, which is an enabling step in the continuous downscaling of the nanometer-sized features characterizing current state-of-the-art chip manufacture.[7] An increasing fraction of these applications requires a vapor-phase preparation method for SiO_2 that is able to operate at relatively low processing temperatures (<350 °C) while yielding excellent material properties with precise thickness control over large substrate areas, often with demanding surface topologies.

Atomic layer deposition (ALD) is a technique capable of meeting these demands as it relies on self-limiting surface reactions between a substrate and separately dosed vapor-phase reactants, typically a precursor and a co-reactant. The self-limiting nature of the reactions enables Ångström-level thickness control with superior uniformity and conformality over large substrate areas.[8] Moreover, to meet the low-temperature requirement necessary for some applications, a plasma can be used as the co-reactant. In this so-called plasma-enhanced ALD (PEALD) approach, the high reactivity of the plasma species allows for deposition at lower temperatures while preserving good material properties.[9] In particular, ALD of SiO_2 generally requires co-reactants such as O_3 and O_2 plasma and, for the specific case of PEALD, SiO_2 films with low-impurity contents have been demonstrated even at room temperature.[10,11] These aspects make PEALD a particularly desired method for the deposition of SiO_2 for several of the aforementioned applications.

Received: September 9, 2021
Revised: October 26, 2021
Published: November 8, 2021

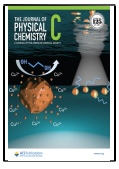

https://doi.org/10.1021/acs.jpcc.1c07980
J. Phys. Chem. C 2021, 125, 24945−24957

Next to the requirements for high-quality films and low-temperature processing, many applications also demand high-throughput processing to ensure commercial viability. This has been driving the increasing interest toward novel fast PEALD concepts. Specifically, in its most conventional approach, PEALD relies on temporally separated gases that are pulsed to a stationary substrate. This configuration, also known as temporal PEALD, is typically performed at a low operating pressure and results in a fairly low throughput. Alternatively, precursor and plasma can be spatially separated and continuously fed to the surface of substrates moving through different zones. This approach is known as spatial PEALD (PE-s-ALD) and allows us to achieve higher throughput values.[12,13] In addition, PE-s-ALD can be performed at atmospheric pressure, which can be desired for applications where cost and volume are highly important, such as (flexible) displays, batteries, and photovoltaic devices.[14−20]

Nowadays, both temporal and spatial low-pressure PEALD processes of SiO_2 are widely employed in commercial manufacturing processes of semiconductor devices. Given its industrial relevance, low-pressure PEALD processes of SiO_2 have been well studied and the understanding of their reaction mechanisms has reached certain maturity. As reviewed in Section 2, this is especially true for the cases using aminosilanes as Si precursors.[7] On the contrary, the atmospheric-pressure PE-s-ALD process of SiO_2 has remained largely unaddressed. It is unexplored how film growth, material properties, and reaction pathways compare to those reported for state-of-the-art low-pressure PEALD of SiO_2. To address these points, it is desirable to gain insight into the underlying chemistry and study how the process conditions affect film growth. Moreover, more knowledge on the atmospheric-pressure PE-s-ALD process of SiO_2 provides a way to evaluate parameters such as throughput and precursor usage efficiency and, therefore, to optimize existing processes according to the specific needs of the application.

In this work, we developed and characterized an atmospheric-pressure PE-s-ALD process for SiO_2 using bisdiethylaminosilane (BDEAS) as the precursor and $Ar-O_2$ plasma as the co-reactant. BDEAS was selected as it is one of the most used aminosilanes for PEALD of SiO_2. Furthermore, it shares many aspects with other aminosilanes,[21] and it can be considered representative of this class of precursors. Within the temperature range of 100−250 °C, we demonstrate that PE-s-ALD growth and material properties are *on par* with the ones reported for low-pressure temporal PEALD. The underlying chemistry was studied with a combination of gas-phase infrared spectroscopy on exhaust gases and optical emission spectroscopy (OES) on the plasma zone. Recently, we employed infrared spectroscopy to characterize the PE-s-ALD process of Al_2O_3 by probing the exhaust plasma gas.[17] Here, we extended this method by analyzing both the precursor and the plasma exhausts, thus identifying the species formed in both half-cycles. Furthermore, the infrared study of the precursor exhaust gas allowed us to quantify the amount of precursor adsorbing on the surface and the byproducts desorbing during the precursor half-cycle. From this quantification, we estimated the precursor depletion for several processing conditions and the number of exchanged ligands per adsorbing precursor molecule. Finally, based on the results, we propose a reaction mechanism of the process.

2. CONCISE OVERVIEW ON THE ALD REACTION MECHANISM OF SIO_2 USING AMINOSILANE PRECURSORS

Low-pressure ALD of SiO_2 has been studied rather extensively for a range of different precursors and co-reactants. A list of the reported SiO_2 ALD processes has been published by Miikkulainen et al.[22] Recently, Ovanesyan et al. have authored a review of the most industrially relevant SiO_2 processes providing an overview on the ALD chemistry for several families of Si precursors,[7] while Fang et al. have reviewed the theoretical modeling studies on ALD of SiO_2.[21] Here, we provide a concise overview on the reaction mechanisms of SiO_2 focusing exclusively on aminosilane precursors and discuss how the chemical structure of the precursor impacts the adsorption behavior and ALD film growth. Furthermore, to provide more context for the mechanistic study presented in this work, we will illustrate the reaction mechanism for the specific case of low-pressure PEALD of SiO_2 using BDEAS and O_2 plasma.

The interest for ALD of SiO_2 as one of the most relevant materials in the semiconductor industry can be traced back to the early 1990s. The two main requirements for SiO_2 films to be implemented in several Si-based technologies were a low thermal budget (<350 °C) during preparation and excellent material quality. ALD of SiO_2 films at temperatures as low as 350 °C was initially demonstrated using $SiCl_4$ and H_2O.[23] However, this specific ALD process presented two main limitations: (i) high-quality SiO_2 films with low chlorine contents could only be obtained at relatively high deposition temperatures (500−600 °C), and (ii) low deposition rates were achieved despite long precursor exposures.[23] In the early 2000s, it was found that pyridine (NC_5H_5) and NH_3 can be used as catalysts for the ALD process of $SiCl_4$ and H_2O, thus enabling high deposition rates while lowering the deposition temperature.[24] Nevertheless, Cl-based precursors are not preferred as they can lead to particle formation and produce HCl as reaction byproduct which is highly corrosive and can undergo further reactions.[24] These limitations made industry move toward Cl-free precursors such as alkoxides, hydrides, and aminosilanes. Yet, alkoxide Si precursors usually suffer from insufficient volatility and low reactivity toward −OH surface groups at low temperatures. SiH_4 is a popular precursor for thin-film deposition of Si-based materials; nevertheless, the strong Si−H bonds hamper the precursor adsorption on −OH surface sites rendering SiH_4 less suitable for SiO_2 deposition.[25,26] In this context, aminosilanes have attracted attention as promising precursor candidates for low-temperature ALD of high-quality SiO_2 films. These precursors have amine ligands which are more reactive toward −OH surface groups compared to chloride- and hydride ligands.[25] The high reactivity of the amine ligands in combination with the use of highly reactive co-reactants such as H_2O_2, O_3, and O_2 plasma has allowed SiO_2 deposition at temperatures lower than 300 °C and, in the specific case of O_2 plasma, even at room temperature.[10,27−33] In addition, aminosilanes are desirable from a safety and operability perspective as they do not lead to the desorption of corrosive reaction byproducts.

Aminosilane precursors are defined by the chemical structures $Si(NR_i)_x(H)_{4-x}$ (with i = 1, 2 and x = 1, 2, 3, 4), where R indicates an alkyl group such as methyl (Me), ethyl (Et) and butyl (*sec*-, *tert*-Bu). They differ from each other by the type of amine and by the ratio of amine ligands $(NR)_x$ to

https://doi.org/10.1021/acs.jpcc.1c07980
J. Phys. Chem. C 2021, 125, 24945−24957

hydride ligands H_{4-x}. Table 1 provides a list of ALD processes of SiO_2 using aminosilanes for which mechanistic insight has been obtained. Despite their structural differences, the adsorption of these precursors on OH-terminated surfaces occurs according to similar reaction pathways where the protonation of amine ligands leads to the production of gas-phase amine compounds as reaction products. This insight into the adsorption behavior has been obtained for several aminosilane precursors by means of both density functional theory (DFT) calculations and infrared absorption spectroscopy experiments. In the case of the mono-aminosilane precursor di(*sec*-butylamino)silane (DSBAS), Huang et al. calculated that the precursor molecule undergoes adsorption through ligand exchange at the surface which results in anchoring of the Si atom together with the formation of surface $-SiH_3$ species and the release of a gas-phase amine byproduct.[34] These theoretical results were confirmed experimentally by Peña et al. who employed infrared adsorption spectroscopy to study DSBAS adsorption on −OH sites and demonstrated the formation of $-SiH_3$ species on the surface after the precursor exposure.[35,36]

Table 1. Overview of Relevant Mechanistic Studies on ALD of SiO_2 Using Aminosilane Precursors

number of amine ligands	precursor	co-reactant	references
1	DMAS (SiH_3NMe_2)	O_2 plasma	3, 18
1	DSBAS ($SiH_3N(sec\text{-}Bu)_2$)	O_3	31, 34, 35, 37
2	BDMAS ($SiH_2[NMe_2]_2$)	O_3, O_2 plasma	21, 25, 26, 38
2	BTBAS ($SiH_2[NH(tert\text{-}Bu)]_2$)	O_3	21, 31, 35, 37, 39, 40
2	BDEAS ($SiH_2[NEt_2]_2$)	O_3, O_2 plasma	4, 11, 25, 37, 40, 41
3	TDMAS ($SiH[NMe_2]_3$)	O_3, H_2O_2	21, 26, 28, 29, 38, 40, 42
4	TKDMAS ($Si[NMe_2]_4$)	H_2O	26, 42

For the case of bis-aminosilane precursors, similar behavior is reported both theoretically and experimentally for bis(*tert*-butylamino)silane (BTBAS), bis(diethylamino)silane (BDEAS), and bis(dimethylamino)silane (BDMAS).[10,35,39,41,43] In particular, for the family of methylaminosilanes, where the alkyl group R is a methyl (dimethylaminosilane (DMAS), BDMAS, tris-(dimethylamino)silane (TDMAS), and tetrakis-(dimethylamino)silane (TKDMAS)), the theoretical work conducted by Jeong et al. has demonstrated that the Si−N is the weakest bond present in the precursor molecules and, therefore, it is the easiest to break in reactions with −OH surface groups during to precursor adsorption.[26] All of these studies indicate that, independently of the number of amine ligands, precursor adsorption for aminosilanes is dominated by the breaking of the Si−N bond.

Concerning the performance of aminosilanes in ALD processing, this is greatly determined by the type and the number of amine ligands contained in their molecular structure. Murray et al. calculated that the nature of the alkyl group (R = Me, Et, Bu) affects precursor adsorption such that the chemisorption of molecules with smaller R groups is energetically more favorable.[25] O'Neill et al. authored a comparative study with focus on the influence of the number of amine ligands on the ALD growth.[40] This study compared the ALD growth and film characteristics for the cases where a tris-aminosilane (TDMAS) and two bis-aminosilanes (BDEAS and BTBAS) were used in combination with O_3 as the co-reactant. The use of TDMAS leads to a reduced deposition rate and to a higher impurity content in the films due to incomplete removal of the amine ligands, especially at low temperatures. These findings are in agreement with a previous report where SiO_2 films containing C and N impurities were deposited using TDMAS and H_2O_2.[42] It was calculated that for bis-aminosilanes, such as BDMAS, BTBAS, and BDEAS, the elimination of both amine ligands during precursor adsorption is possible with the second amine ligand requiring a higher, but still surmountable activation energy.[35,39,43] In contrast to these precursors, for tris-aminosilanes like TDMAS the loss of the third amine ligand is energetically forbidden under typical ALD conditions. Compared to other mono- and bis-aminosilanes, this may lead to more C and N impurities in the film, especially for process conditions where co-reactant dosing does not ensure effective removal of the amine ligands.[38,44] For completeness, it should be mentioned that tetrakis-aminosilane precursors like TKDMAS are found less suitable for ALD growth of SiO_2 due to severe steric hindrance caused by the large amine ligands.[26,42]

The co-reactants used in combination with aminosilanes for low-temperature ALD of SiO_2 are mostly O_3 and O_2 plasma. Both O_3 and O_2 plasma react with the remaining amine ligands at the surface through atomic O species. Specifically, as demonstrated by Dingemans et al. for the case of BDEAS and O_2 plasma, the removal of the amine ligands by the O atoms occurs through combustion-like reactions.[10] Furthermore, O atoms react also with the Si−H bonds at the surface to restore the surface −OH groups that are necessary for the next precursor step.[21,39] These two reaction channels of O atoms with the surface species have been experimentally confirmed by infrared spectroscopy studies on mono-, bis-, and tris-aminosilanes.[28,32,35,42] These works have demonstrated that, during the co-reactant exposure, the SiOH species are regenerated on the surface while CH_x and SiH species are removed.

Bis-aminosilane precursors, in particular BDEAS, can be considered a good representation of the entire class of aminosilanes. BDEAS has a relatively high vapor pressure (4 Torr at 25 °C) which makes it favorable from a precursor delivery point of view. In fact, a high vapor pressure facilitates shorter dosing times which, in turn, shorten the ALD cycle times and increase the throughput. Furthermore, as one of the first aminosilanes that had been explored,[45] BDEAS has been employed in several ALD processes: for SiO_2 using both O_3 and O_2 plasma, for Si_3N_4 using N_2 plasma, and also for ternary materials such as $HfSiO_x$.[10,11,46−48] Moreover, from a mechanistic point of view, the low-pressure PEALD process of SiO_2 from BDEAS and O_2 plasma is one of the most thoroughly studied, theoretically as well as experimentally.[10,11,41] For this particular precursor, Baek et al. calculated that adsorption on −OH surface groups indeed takes place through Si−N bond breaking followed by the protonation of amine ligands $-N(C_2H_5)_2$ to volatile diethylamine molecules ($NH(C_2H_5)_2$, DEA).[41] In a later experimental work, Dingemans et al. used gas-phase diagnostic techniques such as quadrupole mass spectrometry (QMS) and OES to study the PEALD process from BDEAS and O_2 plasma.[10,41,49] They found experimental evidence of DEA desorption during BDEAS adsorption. Moreover, they identified combustion-

https://doi.org/10.1021/acs.jpcc.1c07980
J. Phys. Chem. C 2021, 125, 24945−24957

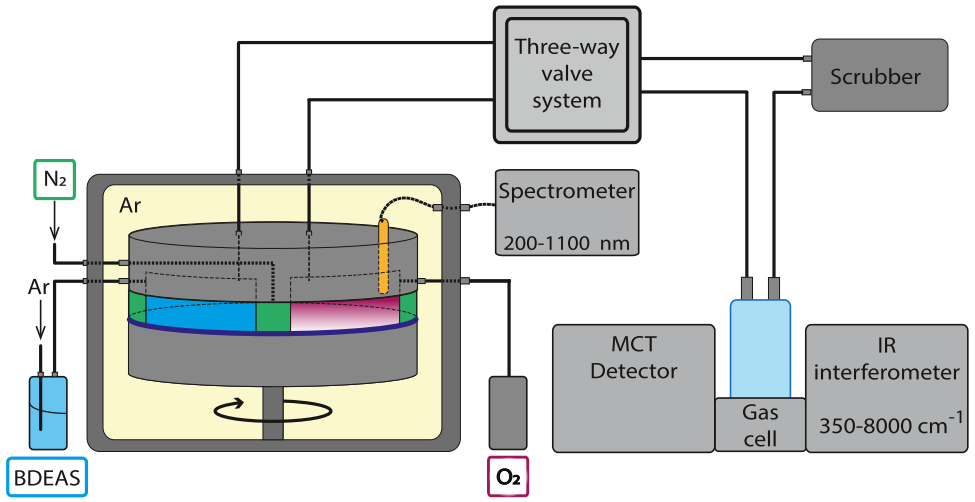

Figure 1. Schematic of the atmospheric-pressure rotary PE-s-ALD reactor. The reactor is placed in an Ar-filled oven and consists of a cylindrical chamber in which the substrate is placed at a 20−250 μm distance from the reactant inlet. The precursor and the plasma exhaust gases are delivered to a gas cell, which is inserted into an IR interferometer. A system of three-way valves allows switching from the precursor to the plasma exhaust such that the reactor gases can be analyzed in a separate manner for both half-cycles. OES is performed by means of a thermally resistant optical fiber connected to a spectrometer and inserted into a transparent plasma source.

like reaction products such as H_2O and CO_2 produced during the plasma half-cycle. This proved that a fraction of the amine ligands remains on the surface after precursor adsorption and that these are then combusted by O_2 plasma species in the co-reactant step. Based on these findings, Dingemans et al. proposed the following chemistry for the process[10]

$$\mathrm{Si{-}OH} + \mathrm{SiH_2[N(C_2H_5)_2]_2} \rightarrow \mathrm{SiO{-}SiH_2[N(C_2H_5)_2]_{2-x}} + x\mathrm{HN(C_2H_5)_2} \quad (1)$$

$$\mathrm{SiH_2[N(C_2H_5)_2]} + \mathrm{O} \rightarrow \mathrm{Si{-}OH} + \mathrm{H_2O} + \mathrm{CO_x} + \text{N-containing species} \quad (2)$$

In reaction 1, BDEAS adsorption proceeds according to the mechanism calculated by Baek et al. in which only a fraction of the amine ligands ($x < 2$) is released in surface reactions under the conditions investigated. In reaction 2, the O atoms in the O_2 plasma combust the remaining amine ligands forming H_2O and CO_x species. The formation of N-containing species was also expected; yet, these products were not directly observed and reaction 2 was therefore left unbalanced. Moreover, O atoms react with the surface Si−H groups by its inserting between the Si and H atoms and forming the surface Si−OH groups that are vital to the BDEAS adsorption in the next ALD cycle.

3. EXPERIMENTAL SECTION

3.1. Deposition Conditions and Material Characterization. SiO_2 films were prepared using the rotary spatial ALD reactor illustrated in Figure 1. Being located in an Ar-filled oven, this cylindrical reactor is composed of a rotating substrate table and a fixed injection head that are separated by a horizontal gap of typically 20−250 μm.[50] The injection head is provided with separated inlets for the precursor and co-reactant vapors. A gas-bearing system providing high flow of N_2 keeps the two vapors separated from each other and from the outside ambient gas. This separation of the reactants creates two half-cycle zones to which the substrate is sequentially exposed during rotation.

In spatial ALD, the exposure time of the substrate to the reactants is defined as the length of the deposition zone divided by the speed of the substrate.[51] In the rotary system used here, the speed of the substrate is determined by the rotation frequency expressed as "rotations per minute" (rpm). Thus, the exposure time is inversely proportional to the rotation frequency. In this configuration, one ALD cycle is achieved after completing a full rotation of the substrate table such that the substrate surface is sequentially exposed to each zone (i.e., precursor, inert gas, co-reactant, and inert gas). To generate the plasma, an atmospheric-pressure dielectric barrier discharge (DBD) plasma source with an alumina dielectric was used.[52]

SiO_2 films were deposited on Si wafers using bisdiethylaminosilane (BDEAS) as the silicon precursor and Ar−O_2 plasma as the co-reactant. The BDEAS precursor was contained in a bubbler kept at 20 °C. A pickup flow of Ar through the bubbler is used to dose BDEAS to the chamber. The Ar flow was controlled using a mass-flow-controller (MFC) and varied between 0.01 and 0.2 slm which corresponded to actual BDEAS flows ranging from 1.5×10^{-5} to 3.0×10^{-4} slm. Section S1 in the Supporting Information describes the calculation of the actual BDEAS flow to the chamber and provides values corresponding to the Ar pickup flows used. Once extracted from the bubbler, the Ar and BDEAS are further diluted by additional Ar such that a total flow of 1 slm is reached and a constant flow is ensured. The BDEAS/Ar gas mixture is transported to the chamber through stainless steel lines heated to 100 °C. For the Ar−O_2 plasma feed gas, the Ar flow was kept constant at 2.8 slm, while the O_2 flow was varied between 0 and 0.1 slm. During film deposition, the exposure time of the substrate surface to the reactants was varied between 40 and 400 ms by setting the rotation speed between 100 and 10 rpm, respectively. The deposition temperature was varied between 100 and 250 °C by setting the temperature of the oven. Before each deposition, the substrate was exposed to a 2 min Ar−O_2 plasma cleaning step.

https://doi.org/10.1021/acs.jpcc.1c07980
J. Phys. Chem. C 2021, 125, 24945−24957

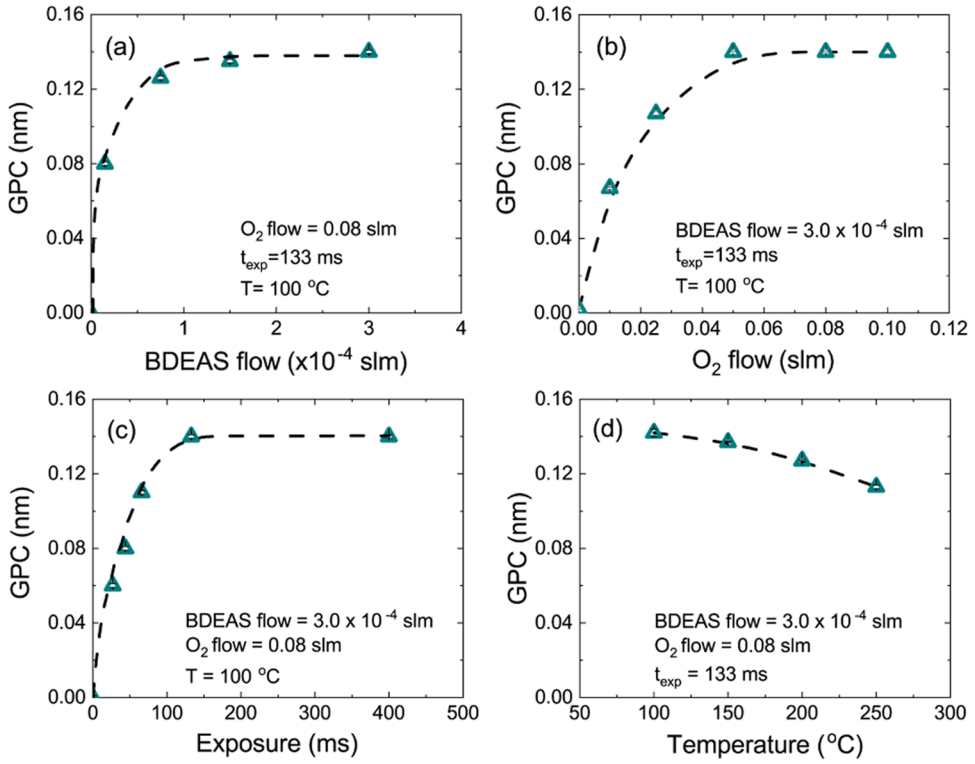

Figure 2. Growth per cycle (GPC) as a function of (a) BDEAS flow, (b) O_2 flow, (c) exposure time (all for 100 °C), and (d) deposition temperature. The dotted lines are a guide to the eye.

Ex situ spectroscopic ellipsometry (SE) was used to measure the thickness and the refractive index of the SiO_2 layers. The SE analysis was performed with a J.A. Woollam M2000 spectrometer fitting the data with a Cauchy model. From the thickness data, the growth per cycle (GPC) was calculated. The values of the refractive index were determined at 632 nm.

The chemical composition of the films was determined by Rutherford backscattering spectroscopy (RBS) and elastic recoil detection (ERD) which were performed by Detect99 using a Singletron system with a 3 MeV He^+ beam. Stoichiometry, hydrogen content, and the number of Si atoms deposited per nm^2 per cycle were determined from the RBS/ERD results, while the mass density was calculated by combining RBS/ERD and SE data.

3.2. Spectroscopic Characterization of the Process. Gas-phase infrared absorption spectroscopy on effluent gases and OES on the plasma region were used to study the atmospheric-pressure PE-s-ALD process of SiO_2 at a deposition temperature of 100 °C. Both spectroscopic techniques were implemented on the reactor as shown in Figure 1.

Gas-phase infrared spectroscopy was performed by means of a gas cell inserted into the sample compartment of a Bruker Vertex70 Fourier Transform Infrared (FTIR) interferometer. The exhausted gases were fed into the gas cell through stainless steel lines. The exhaust precursor and co-reactant gases could be analyzed separately by means of a three-way valve system, which allows switching from one exhaust to the other. Before starting the data acquisition, the gas cell was purged for two hours with 7 slm of N_2 to achieve a stable, air-free background. For the analysis of the precursor exhaust gas, data were acquired in the "precursor only" mode and the "precursor half-cycle" mode. In the "precursor only" mode, only BDEAS is delivered to the system without the plasma being activated. In the "precursor half-cycle" mode, BDEAS is supplied with the plasma switched on to run the ALD process. For the analysis of the plasma exhaust gas, data were acquired in "plasma only" mode and "plasma half-cycle" mode. In the "plasma only" mode, the plasma is activated without supplying BDEAS. In the "plasma half-cycle" mode, the plasma is on and the BDEAS is supplied so that the ALD process takes place. After switching from the precursor to the plasma exhaust analysis, the gas cell was purged for 3 min with a flow of 1 slm of Ar to eliminate residual gases from the previous step.

Each infrared spectrum was acquired using a resolution of 0.5 cm^{-1} and a collection time of 600 s. To distinguish between the dominant signal from the precursor and the signal from the reaction byproducts, two different BDEAS flow settings were used for the analysis of the precursor and the plasma exhaust, respectively 7.5×10^{-5} and 3.0×10^{-4} slm. This choice is explained in Section S2 in the Supporting Information.

The infrared signature of DEA was measured in a dedicated experiment since DEA is likely to be produced as the main reaction byproduct during BDEAS adsorption. For this experiment, a flow of DEA was fed into the gas cell. To dose DEA into the gas cell, an Ar pickup flow of 0.025 slm was introduced into the DEA bubbler kept at room temperature. The infrared spectrum was acquired using a resolution of 0.5 cm^{-1} and a collection time of 600 s.

The OES study was carried out with a thermally resistant optical fiber coupled to a specially designed DBD plasma source with a quartz dielectric and a top electrode made of a combination of Ag and indium tin oxide (ITO). This configuration provides a direct view to the plasma region through the ITO-covered quartz. The optical fiber was

https://doi.org/10.1021/acs.jpcc.1c07980
J. Phys. Chem. C 2021, 125, 24945−24957

connected to an Avantes spectrometer (AvaSpec-ULS2048x16) with a resolution of 0.5 nm. In line with the FTIR experiments on the plasma exhaust, the OES spectra were recorded in "plasma only" mode and "plasma half-cycle" mode. The BDEAS flow was set to 3.0×10^{-4} slm. For each spectrum, an integration time of 12 s was used.

4. RESULTS

4.1. Film Growth and Material Characteristics. For the development of the PE-sALD process, the ALD saturation behavior was measured at a fixed rotation speed for different flows of the precursor and co-reactant. Specifically, when varying the precursor flow, the co-reactant flow was kept constant, and vice versa. Figure 2 shows the effects of BDEAS flow, O_2 flow, exposure time, and temperature on the growth per cycle (GPC) of the SiO_2 films.

In the rotary ALD system, the exposure time sets the duration of all of the process steps within one cycle, i.e., precursor dosing, plasma exposure, and purging. In order not to be limited by subsaturation due to insufficient dosing of the reactants, a relatively long exposure time of 133 ms (corresponding to a rotation frequency of 30 rpm) was chosen when varying the flows of precursor and co-reactant; in a similar way, relatively high flows were chosen when varying the exposure time. The data in Figure 2a−c were acquired at a temperature of 100 °C. At this temperature and using an exposure time of 133 ms, we found that a BDEAS flow of 1.0×10^{-4} slm and an O_2 flow of 0.05 slm are sufficient to achieve saturation with a GPC of 0.14 nm. Upon further optimization, the effects of rotation speed and deposition temperature on the GPC were explored. In Figure 2c, a BDEAS flow of 3.0×10^{-4} slm and an O_2 flow of 0.08 slm were used while varying the exposure time. The GPC saturates again at 0.14 nm for exposures longer than 133 ms. The dependence of the GPC on the deposition temperature is shown in Figure 2d. For each temperature, the depositions were performed at earlier established saturation conditions using a BDEAS flow of 3.0×10^{-4} slm, an O_2 flow of 0.08 slm, and an exposure time of 133 ms. Upon increasing the temperature, the GPC decreases from 0.14 nm at 100 °C to 0.12 nm at 250 °C. Our GPC values are in good agreement with the ones previously reported for the low-pressure cases where O_2 plasma and O_3 were used as the co-reactants.[10,46]

The film properties of the SiO_2 layers were analyzed for different deposition temperatures and under saturated growth conditions. The results are given in Figure 3. An H content of 9 at. % was found at each temperature, while C- and N-contents were below the detection limits for RBS (<2 at. %). The O- and Si-contents correspond to an [O]/[Si] ratio of 2.1 which points to slightly O-rich films. The refractive index of 1.46 and the density of 2.1 g/cm^3 remain largely constant with temperature. Overall, our data are in line with those reported for low-pressure PEALD of SiO_2 by Dingemans et al. who also found that the material properties were relatively independent of the deposition temperature within the range 100−250 °C.[10] The number of Si atoms deposited per nm^2 per cycle decreased from 3 to 2.5 with increasing temperature. These GPC values are slightly higher than the values reported by Dingemans et al. for the low-pressure PEALD case, decreasing from 2.8 ± 0.1 to 2.1 ± 0.1 Si atoms per nm^2 per cycle when increasing the temperature from 100 to 300 °C.[10]

A decrease of the GPC at higher temperatures is often observed for ALD of oxides.[53,54] A temperature increase induces dehydroxylation which results in a reduced density of −OH surface groups that can act as reactive sites, thus leading to less BDEAS adsorption. This explains the lower number of Si atoms deposited per nm^2 per cycle at higher temperatures as well as the lower GPC shown in Figure 2a. Furthermore, we attribute the H content predominantly to the incorporation of OH groups in the films. The presence of −OH most likely also explains the slightly over-stoichiometric [O]/[Si] ratio indicating an excess of oxygen in the films. The absence of detectable levels of C and N in the films suggests a virtually complete removal of the $-N(C_2H_5)_2$ ligands after the plasma step.

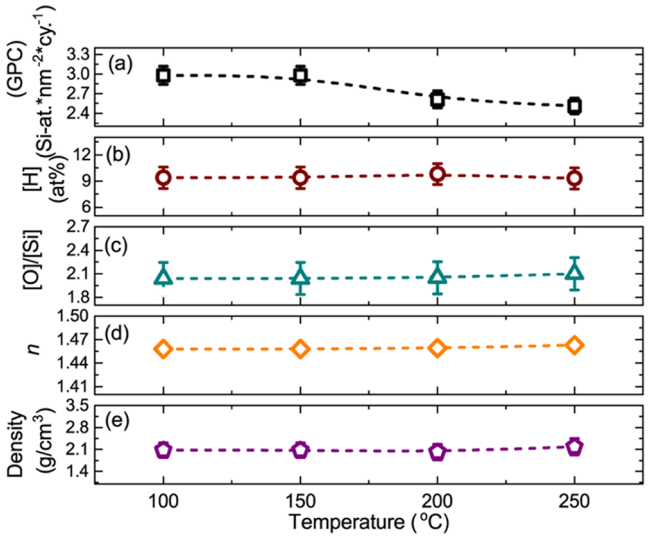

Figure 3. GPC and material properties of the SiO_2 films as a function of deposition temperature: (a) GPC in terms of Si atoms deposited per nm^2, (b) H content [H], (c) [O]/[Si] ratio, (d) refractive index n, and (e) mass density of the films. These parameters were determined by RBS, ERD, and SE.

4.2. Spectroscopic Analysis of the Deposition Process. *4.2.1. Gas-Phase Infrared Spectroscopy.* The gas-phase species produced during the two half-cycles were measured by infrared absorbance spectroscopy on the exhaust gases of both reactants. Figure 4 displays the results obtained for the precursor exhaust. The observed vibrational frequencies with assigned chemical species are listed in Table 2 and have been previously identified elsewhere.[42,55] In Figure 2, we marked only selected vibrational modes that are most relevant for the discussion.

The "precursor half-cycle" spectrum in Figure 4a is characterized by peaks originating from both the precursor and reaction byproducts produced during BDEAS adsorption. The "precursor only" spectrum in Figure 4b is obtained by deactivating the plasma while supplying only the precursor. At the temperatures considered in this work, BDEAS vaporizes without chemically decomposing[57] and, therefore, Figure 4b corresponds to the infrared fingerprint spectrum of the precursor. By comparing Figure 4a and b, it can be seen that the "precursor half-cycle" spectrum exhibits several vibrational modes that are only characteristic of the precursor molecule, such as the Si−N−C stretching and the Si−H stretching. In Figure 4a, these peaks show a reduced absorbance compared to the BDEAS fingerprint spectrum, thus pointing to precursor consumption in ALD reactions. Furthermore, the "precursor half-cycle" spectrum presents additional infrared vibrational

https://doi.org/10.1021/acs.jpcc.1c07980
J. Phys. Chem. C 2021, 125, 24945−24957

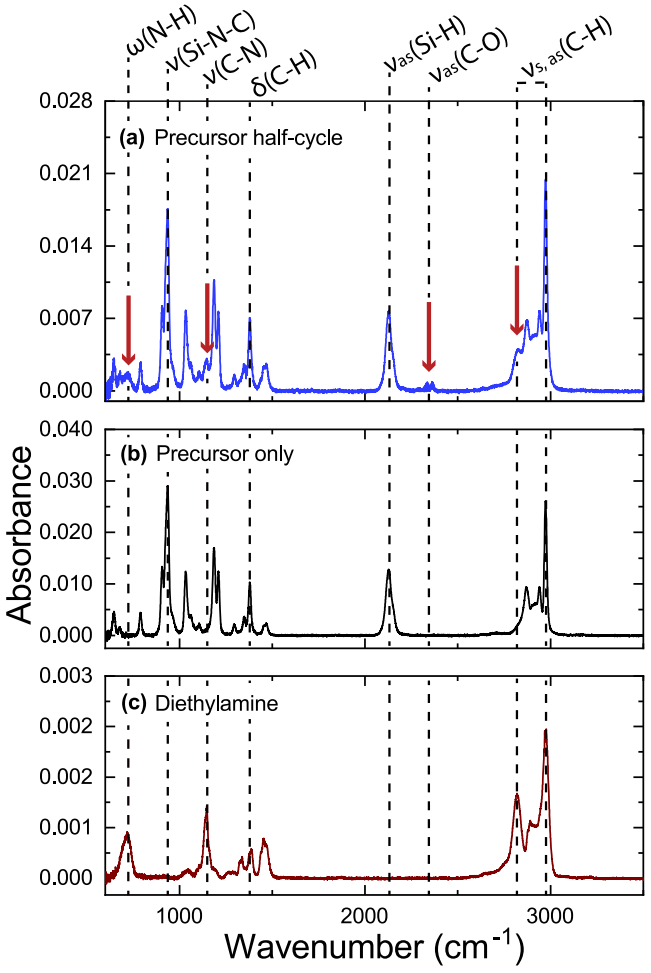

Figure 4. Infrared spectra of the exhaust precursor gas obtained in (a) "precursor half-cycle" mode, (b) "precursor only" mode, and (c) the spectrum of diethylamine (DEA). The "precursor only" and "precursor half-cycle" spectra were acquired at a temperature of 100 °C using a BDEAS flow of 7.5×10^{-5} slm and an exposure time of 40 ms. Selected vibrational peaks have been assigned. In the "precursor half-cycle" spectrum, the absorbance peaks corresponding to desorbing reaction products have been indicated for convenience.

modes at 727, 1047, and 2880 cm^{-1}. The comparison of the "precursor half-cycle" spectrum (Figure 4a) with the DEA fingerprint spectrum in Figure 4c reveals that these additional peaks can be assigned to the characteristic N−H wagging, C−N stretching, and C−H stretching modes of the DEA molecule.[58] These results indicate that DEA is produced as a main reaction product during precursor adsorption.[10,21,41]

Additionally, in the "precursor half-cycle" spectrum, the asymmetric stretching mode of CO_2 is identified (~2350 cm^{-1}). The production of CO_2 during the precursor half-cycle was not expected; however, upon closer inspection, it appears that it is not uncommon in PEALD of oxides. In fact, it has been previously reported that CO_2 production during precursor adsorption is directly related to the use of a plasma as the co-reactant, and it will be addressed later in more detail.[59,60]

Figure 5 shows the infrared absorption spectra obtained by probing the exhaust gases of the plasma zone. The observed vibrational frequencies with assigned chemical species characterizing the plasma half-cycle are also listed in Table 2. The "plasma half-cycle" spectrum in Figure 5a is characterized by the vibrational modes associated with species formed within the O_2 plasma as well as reaction products created during the co-reactant step. In this spectrum, we identify O_3, H_2O, CO_2, CO, N_2O, NO_2, and CH-containing species. The plasma only spectrum in Figure 5b displays two peaks at 1041 and 2100 cm^{-1} which are attributed to the asymmetric stretching vibrational mode of O_3 and its overtone. A comparison between the two spectra shows that O_3 is produced in the O_2 plasma itself,[17,61] whereas the remaining species in Figure 5a are created upon reactions of plasma species with the precursor ligands present at the surface. In particular, the absorbance from CO_2 and H_2O indicates that the oxygen atoms react through combustion-like reactions with the $-N(C_2H_5)_2$ ligands.[10]

The presence of NO_2 and N_2O suggests reactions of O atoms with the N that is present in the $-N(C_2H_5)_2$ ligands. Although their production can be expected when using an aminosilane precursor,[10] the formation of such species in PEALD of SiO_2 has not been experimentally observed before.

Table 2. Vibrational Frequencies Observed during the Precursor Half-Cycle for the Deposition of SiO_2 Using BDEAS and O_2 Plasma

	wavenumber (cm^{-1})	band assignment	assigned species	references
precursor half-cycle	645−936	Si−N−C stretching (ν)	BDEAS	42, 55, 56
	727	N−H wagging (ω)	DEA	57
	1030−1207	C−N stretching (ν)	BDEAS/DEA	42, 55−57
	1147	C−N stretching (ν)	DEA	57
	1290−1463	C−H_x bending (δ)	BDEAS/DEA	42, 55−57
	2100	Si−H_2 sym. stretching (ν_s)	BDEAS	42, 55, 56
	2350	C−O asym. stretching (ν_{as})	CO_2	60
	2870−2973	C−H_x sym/asym stretching ($\nu_{s,as}$)	BDEAS/DEA	42, 55−57
precursor half-cycle	1041	O−O−O asym. stretching (ν_{as})	O_3	61
	1611	N−O asym. stretching (ν_{as})	NO_2	61
	1622	O−H−O sym. bending (δ_s)	H_2O	60
	2100	asym. stretching overtone (ν_{as})	O_3	61
	2140	C−O stretching (ν)	CO	60
	2250	N−O sym. stretching (ν_s)	N_2O	61
	2350	C−O asym. stretching (ν_{as})	CO_2	60
	3000	C−H_x asym./sym. stretching ($\nu_{s,as}$)	CH-species	
	3755	O−H asym./sym. stretching ($\nu_{s,as}$)	H_2O	60

https://doi.org/10.1021/acs.jpcc.1c07980
J. Phys. Chem. C 2021, 125, 24945−24957

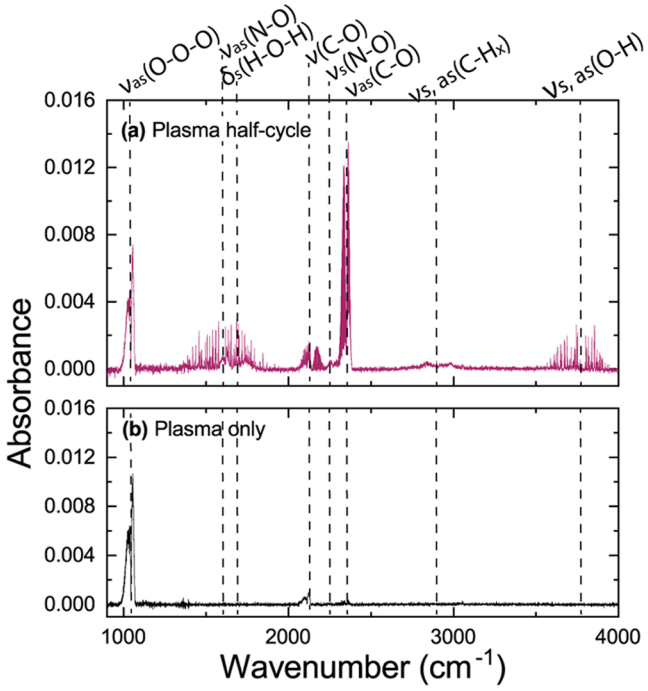

Figure 5. Infrared spectra of the exhaust plasma gas obtained in (a) "plasma half-cycle" mode and (b) "plasma only" mode. The spectra were acquired at a temperature of 100 °C using a BDEAS flow of 3.0 × 10^{-4} slm and an exposure time of 40 ms.

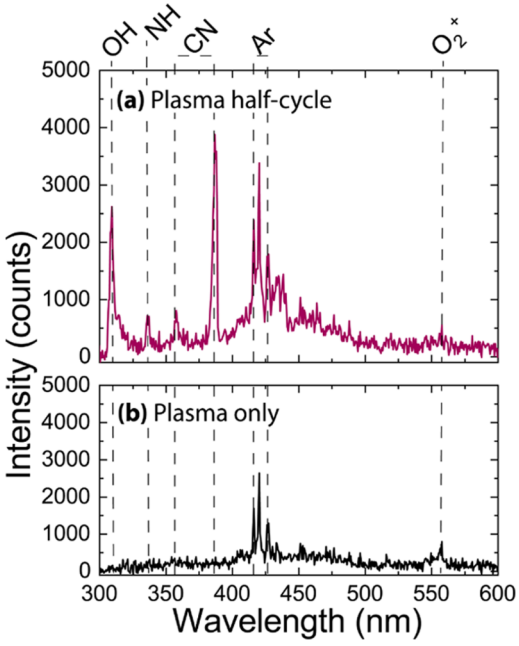

Figure 6. OES spectra of the plasma region obtained in (a) "plasma only" mode and (b) "plasma half-cycle" mode at a temperature of 100 °C, a BDEAS flow of 3.0 × 10^{-4} slm, and an exposure time of 40 ms.

The reactions producing these species can be surface reactions as well as reactions in the plasma gas phase. In the first case, O atoms react directly with the amine ligands at the surface in a combustion-like reaction pathway. In the second case, O atoms react with N-containing species that have been released into the plasma upon surface reactions. For instance, it can be speculated that O and O-containing species react with the N present in the plasma to form NO, NO_2, and N_2O. Such reaction pathways have been often reported for DBD plasmas based on a N_2−O_2 mixture.[62,63]

Finally, the weak infrared absorbance signal around 2900 cm^{-1} by the C−H stretching mode points to the presence of hydrocarbons. These species can originate from incomplete combustion of the amine ligands at the surface or can be formed in subsequent gas-phase reaction pathways, where O atoms react with the ethyl groups that are released in the plasma.

4.2.2. Optical Emission Spectroscopy. Figure 6 shows the excited species in the plasma for the "plasma half-cycle" and "plasma only" modes as studied by OES. Similar to the infrared experiments, the two spectra display differences that are due to the reaction products formed during ligand removal. In the "plasma half-cycle" spectrum, we identified the OH ($A^2\Sigma^+ \rightarrow X^2\Pi$) emission band centered at 309 nm and the NH ($A^3\Pi \rightarrow X^3\Sigma$) emission band at 336 nm, and the violet system of CN ($B^2\Sigma \rightarrow A^2\Pi$) with emission lines at 358 and 380 nm. The so-called first negative system (FNS) of the oxygen O_2^+ ($b^4\Sigma_g^- \rightarrow a^4\Pi_u$) at 557.8 nm, O_2^+ emission at 557.8 nm, and emission lines from ionized Ar in the range of 416−426.3 nm are observed in both spectra.[17]

By comparing the two spectra, it can be seen that the intensity of the O_2^+ emission decreases during the plasma half-cycle. This is in line with the fact that oxygen species are consumed in surface reactions with the precursor ligands. The emission from OH, NH, and CN excited fragments are only present in the "plasma half-cycle" spectrum, indicating that these species are formed during the removal of the ligands from the surface. In fact, reaction products are released into the plasma and can undergo excitation reactions by electron impact. Subsequently, emission originates from radiative de-excitation of these excited species. In this scenario, the OH emission most likely originates from electron-impact dissociation of H_2O molecules according to

$$H_2O + e^- \rightarrow OH^* + H + e^- \quad (3)$$

In reaction 3, the H_2O is predominantly produced by combustion of the precursor ligands. OH emission during the plasma co-reactant step was also observed in the case of low-pressure PEALD of SiO_2 and for other low-pressure and atmospheric-pressure PEALD processes of oxides.[10,17,64,65]

The emission from NH and CN excited species was not observable at low pressure for the SiO_2 process,[10] but in our case, these emission bands can originate from electron impact dissociation of ligands or their fragments. As N is released in the plasma during ligand removal from the surface, the formation of N-containing excited species can be expected for PEALD of oxides where an amine precursor is used.[64]

5. DETAILED ANALYSIS OF THE PRECURSOR ADSORPTION STEP

5.1. CO_2 Formation during Precursor Adsorption. The infrared spectrum obtained in the "precursor half-cycle" mode and displayed in Figure 4a shows a weak signal due to CO_2. As the BDEAS molecule does not contain O atoms, CO_2 formation upon precursor adsorption is not readily expected. We attribute the observation of CO_2 to the presence of surface carbonate groups (CO_3^{2-}) which are created during the O_2 plasma step. These carbonates are released from the surface during the adsorption of BDEAS molecules in the subsequent cycle, leading to CO_2 as the reaction product. This mechanism

https://doi.org/10.1021/acs.jpcc.1c07980
J. Phys. Chem. C 2021, 125, 24945−24957

was previously proposed by Rai et al. for PEALD of Al_2O_3 and TiO_2 using trimethylaluminum (TMA) and titanium isopropoxide (TTIP), respectively.[59,60] By studying the surface species by infrared absorbance spectroscopy, it was demonstrated that carbonates are formed as intermediate surface groups during the co-reactant step and removed in the subsequent precursor adsorption accompanied by CO_2 production.

To validate our hypothesis, we investigated the effect of exposure time and temperature on the production of CO_2 and the results are presented in Section S3 in the Supporting Information. Figure S4 shows that the production of CO_2 decreases with increasing plasma exposure. Specifically, shorter plasma exposures are not sufficient to drive the reaction to completion by decomposing all surface carbonates, thus leading to more CO_2 being produced during BDEAS adsorption. This is in line with the work of Rai et al., which also showed that prolonged plasma exposures lead to a lower surface density of these intermediates.[59,60]

Figure S5 shows that the peak intensity of CO_2 in the absorbance spectrum is higher at 100 °C than at 250 °C. This indicates that at lower temperatures, there is a higher density of these intermediates leading to more CO_2 desorbing upon precursor adsorption. These findings are in agreement with previous works reporting that the density of intermediate carbonaceous species such as carbonates and formates on oxide surfaces decreases with temperature.[59,60,66]

5.2. Quantitative Analysis of Precursor Adsorption. *5.2.1. Determination of Precursor Depletion.* The precursor depletion is defined as the fraction of the initially introduced precursor that has been consumed in ALD reactions. This quantity can be calculated from the infrared absorbance spectra obtained by monitoring the precursor exhaust gas. Under condition of constant flow and applying the Beer−Lambert law, the absorbance can be considered proportional to the flow of species. In our case, with the total flow of the precursor to the chamber being constant, it is reasonable to assume that the absorbance of the peaks originating from the BDEAS molecule is proportional to the flow of BDEAS through the gas cell. This assumption allows us to calculate the BDEAS depletion based on the Si−H stretching mode at 2100 cm^{-1} peak as this vibrational mode is only representative of the BDEAS molecule. The BDEAS depletion can be extracted from

$$\text{BDEAS depletion} = 1 - \frac{A(\text{Si}-\text{H})}{A(\text{Si}-\text{H})_0} \times 100\% \quad (4)$$

with $A(Si-H)_0$ and $A(Si-H)$ being the integrated absorbance of the Si−H peak in "precursor only" and "precursor half-cycle" modes, respectively. Subsequently, using eq 4, the flow of BDEAS that has reacted can be calculated by multiplying the precursor depletion by the precursor flow. See Section S4 in the Supporting Information for the uncertainty analysis.

The precursor depletion can be used to rate the process performance for several process parameters. Ideally, conditions of high precursor flows and long exposures ensure working under fully saturated conditions. However, they also lead to an inherently higher quantity of unreacted precursor and, therefore, may not be preferred from a manufacturability point of view. In Figure 7, we show the BDEAS depletion for two different BDEAS flows as a function of the exposure time. In the same graph, we also show the GPC for the higher BDEAS flow and the deposition rate calculated as the deposited thickness per unit of time. Figure 7a reveals a

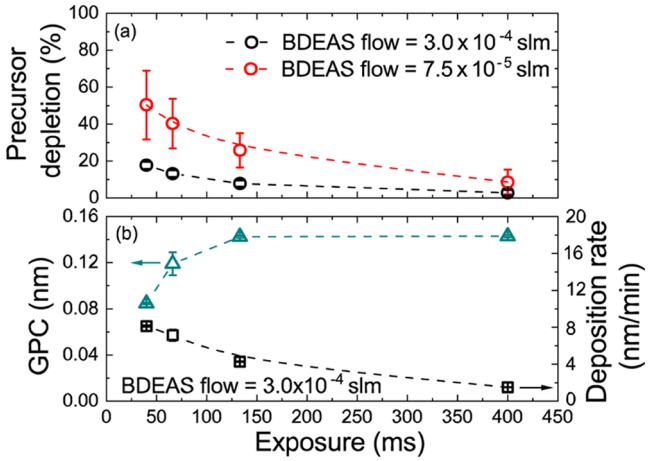

Figure 7. (a) BDEAS depletion for two BDEAS flows as determined from the infrared spectroscopic data for different exposure times. (b) GPC of the SiO_2 films as well as deposition rate (in terms of the amount of material deposited per minute), both as a function of the exposure time and for a BDEAS flow of 3.0×10^{-4} slm.

higher precursor depletion, up to 50%, when using a lower BDEAS flow (7.5×10^{-5} slm) and, for both flow conditions, the depletion decreases with increasing exposure time. For the case of the higher BDEAS flow, Figure 7b illustrates that the deposition rate decreases with exposure time. As the deposition rate shows the same trend as the depletion, all of the depleted BDEAS is actually utilized in surface ALD reactions and converted into a film (see also Section S5 in the Supporting Information).

Figure 7 shows that process conditions corresponding to undersaturated growth yield higher depletion values. When the precursor dosing (i.e., precursor flow times exposure time) is not sufficient, the process is in a precursor-limited regime and the growth is not saturated. Non-saturated growth is obtained for lower BDEAS flows at a fixed exposure and for lower exposure times at a fixed flow. In these two cases, most of the precursor is utilized in ALD reactions to reach full surface saturation, whereas the fraction of unreacted precursor is minimal.

5.2.2. Quantification of the Number of Exchanged Ligands. The N−H wagging mode at 727 cm^{-1} in the "precursor half-cycle" spectrum of Figure 4a was used to quantify the DEA molecules desorbing from the surface during the precursor half-cycle (see explanation in Section S6 in the Supporting Information). The ratio of desorbed DEA molecules to adsorbed (i.e., reacted) BDEAS molecules is plotted in Figure 8 as a function of the exposure time for the two BDEAS flows considered earlier. (We excluded the data measured at 400 ms because of their poor signal-to-noise ratio). This analysis provides an average ratio of desorbed DEA to adsorbed BDEAS of 1.1 ± 0.1. Despite considerable scatter in the data, this result reveals that approximately one DEA molecule is produced per adsorbing BDEAS molecule. Hence, it can be concluded that, on average, BDEAS molecules adsorb on OH surface sites through the exchange of one amine ligand (see Section 2). After BDEAS adsorption, the other amine ligand remains on the surface and is, then, combusted by the O_2 plasma in the co-reactant step.

5.3. Proposed Reaction Mechanism for Atmospheric-Pressure PE-s-ALD for SiO_2. Based on the data presented in this work, we will now summarize the insights obtained on the

https://doi.org/10.1021/acs.jpcc.1c07980
J. Phys. Chem. C 2021, 125, 24945−24957

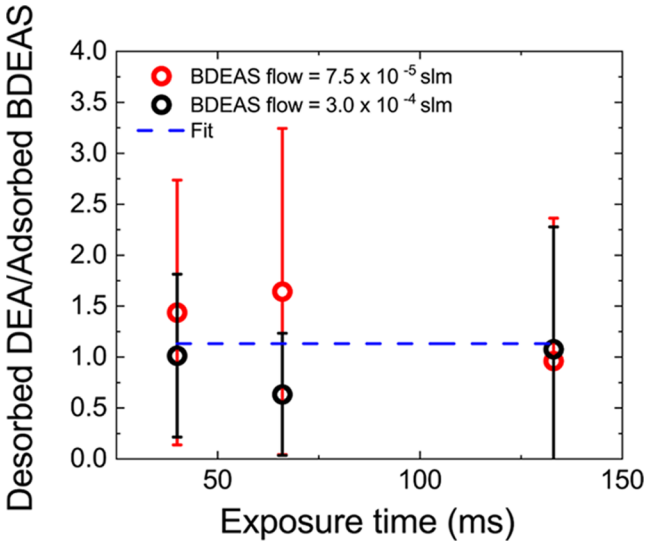

Figure 8. Ratio of desorbed DEA molecules to reacted BDEAS molecules during the precursor half-cycle plotted as a function of the exposure time and for two values of the BDEAS flow. The dotted line represents the average value.

deposition of SiO_2 by atmospheric-pressure PE-s-ALD from BDEAS and Ar−O_2 plasma. Figure 9 provides a schematic representation of the proposed reaction mechanism. Here, we neglected the formation of CO_2 as a byproduct during the precursor step.

BDEAS molecules adsorb on −OH groups through ligand exchange in which the Si−N bond is broken and $-N(C_2H_5)_2$-ligands are protonated to form volatile DEA ($HN(C_2H_5)_2$). We found evidence that precursor adsorption occurs through the exchange of on average one amine ligand per BDEAS molecule. The loss of the second amine ligand appears less energetically favorable.[35,39,43] Therefore, the following reaction is proposed for the precursor adsorption

$$(SiO_2)-OH + SiH_2[N(C_2H_5)_2]_2 \rightarrow (SiO_2)-O-SiH_2[N(C_2H_5)_2] + HN(C_2H_5)_2 \quad (5)$$

Here, the notation $(SiO_2)-OH$ refers to surface hydroxyl groups on the SiO_2 surface that act as reaction sites for the incoming BDEAS molecules. Reaction 5 implies that at the end of the precursor half-cycle, the substrate surface is covered with $-N(C_2H_5)_2$ and −H ligands.

As co-reactant, the O_2 plasma is composed of several reactive species that include O radicals and O_3 molecules, the latter being abundantly created in atmospheric-pressure O_2 plasmas.[17] During the plasma half-cycle, the highly reactive O atoms react with the surface and remove the $-(N(C_2H_5)_2)_2$ ligands. Moreover, O atoms react with hydride ligands by inserting into the Si−H bonds.[10,42,64] Based on our results, the following simplified reaction is proposed for the plasma half-cycle

$$(SiO_2)-O-SiH_2[N(C_2H_5)_2] + 16O \rightarrow (SiO_2)=Si(OH)_2 + 5H_2O + 4CO_2 + NO_2 \quad (6)$$

Here, the notation $(SiO_2)=Si(OH)_2$ is intended to represent a Si atom with two backbonds to the SiO_2 film and terminated by two hydroxyl surface groups.

The removal of the amino ligands occurs mainly through combustion-like reactions initiated by oxygen species and leading to the desorption of H_2O, CO_2, and NO_2 as the main byproducts. Next to full-combustion products in reaction 6, CO, N_2O, and CH-containing species are also produced. CO is likely to be produced in incomplete combustion reactions of the amine ligands or by electron-induced dissociation of CO_2 molecules in the plasma.[67] N_2O can also be created in incomplete combustion reactions at the surface or in further gas-phase reactions involving NO_2 molecules. We speculate that the CH-containing species are mostly formed from fragments of amine ligands that desorb from the surface upon plasma exposure. The emission from CN* and NH* excited species confirms that volatile fragments of amine ligands are indeed present in the plasma. These excited species as well as OH* are most likely originating from electron-induced dissociation reactions of reaction products in the plasma.

Reaction 6 illustrates a simplified scenario which is in line with results from DFT studies and which assumed that O_2 plasma leaves the surface covered with geminal silanol groups ($=Si(OH)_2$), where the Si atom is bound to two back-bonding O atoms.[39,43] The formation of isolated silanol groups ($\equiv$Si−OH), with the Si atom bound to three back-bonding O atoms, is also possible.[53] In agreement with surface infrared

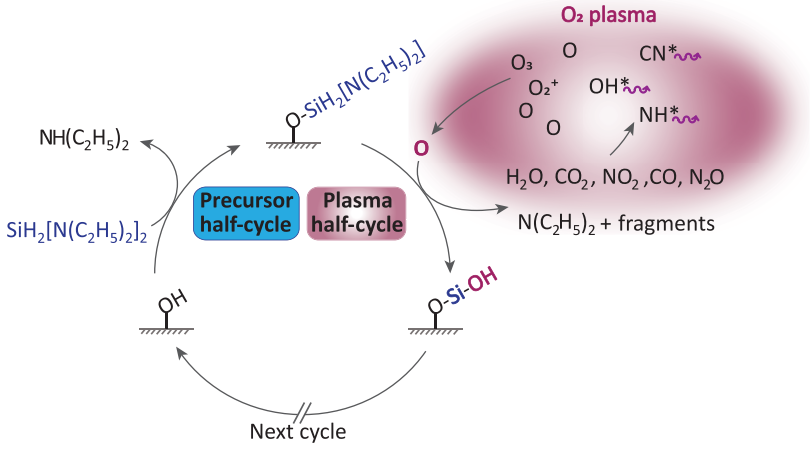

Figure 9. Schematic representation of the reaction mechanism proposed for the atmospheric-pressure PE-s-ALD process of SiO_2 from BDEAS and Ar−O_2 plasma.

https://doi.org/10.1021/acs.jpcc.1c07980
J. Phys. Chem. C 2021, 125, 24945−24957

spectroscopy studies reported earlier,[35,42] the insertion of O atoms into the Si−H bonds upon co-reactant exposure ensures restoration of the −OH surface groups such that precursor adsorption can continue in the next ALD cycle.

6. CONCLUSIONS

Atmospheric-pressure PE-s-ALD of SiO_2 films using BDEAS and Ar−O_2 plasma was demonstrated and self-limiting growth was confirmed within the temperature range of 100−250 °C. The SiO_2 material properties, such as refractive index, atomic composition, and mass density, were in good agreement with the previously reported values for the low-pressure PEALD case.

Infrared absorbance spectroscopy on reactor exhaust gases enabled the identification of the gas-phase species formed in the two half-cycles. Specifically, this analysis revealed that diethylamine (DEA) and CO_2 are formed as reaction byproducts during the precursor half-cycle, whereas in the plasma half-cycle, products such as H_2O, CO_2, NO_2, CO, N_2O, and CH-containing species are created. In addition to infrared spectroscopy, OES measurements during the plasma half-cycle revealed the presence of OH*, CN*, and NH* excited species in the plasma.

It was proposed that CO_2 production during BDEAS adsorption is related to intermediate surface carbonates created during the plasma step. From a quantitative analysis of the precursor adsorption, a higher precursor depletion was found for those processing conditions yielding a subsaturation of the precursor step and a maximum value of 50% could be derived for the precursor depletion. Moreover, from the quantification of the desorbing reaction product DEA, it was calculated that on average, one amine ligand per BDEAS molecule is exchanged during BDEAS adsorption.

Based on the results, a simplified reaction mechanism for the atmospheric-pressure PE-s-ALD of SiO_2 was proposed. BDEAS molecules adsorb on −OH surface sites by exchanging one amine ligand per molecule and releasing DEA as the main byproduct. After precursor adsorption, the surface is covered with hydrides and the remaining amines. These amine ligands are combusted by the plasma species to H_2O, CO_2, and NO_2. Next to these full-combustion products, CO, N_2O, and CH-containing species are created in surface and gas-phase reactions of O_2 plasma species with amine ligands and fragments thereof. Furthermore, the gas-phase species released in the plasma can undergo electron-induced excitation reactions to form OH*, CN*, and NH* excited fragments. After the plasma half-cycle, the −OH groups needed for BDEAS adsorption are restored.

■ ASSOCIATED CONTENT

Supporting Information

The Supporting Information is available free of charge at https://pubs.acs.org/doi/10.1021/acs.jpcc.1c07980.

Additional experimental details including uncertainty calculations and graphs (PDF)

■ AUTHOR INFORMATION

Corresponding Author

W. M. M. Kessels − *Department of Applied Physics, Eindhoven University of Technology, 5600 MB Eindhoven, The Netherlands;* orcid.org/0000-0002-7630-8226; Email: w.m.m.kessels@tue.nl

Authors

M. A. Mione − *Department of Applied Physics, Eindhoven University of Technology, 5600 MB Eindhoven, The Netherlands;* orcid.org/0000-0003-1376-1565

V. Vandalon − *Department of Applied Physics, Eindhoven University of Technology, 5600 MB Eindhoven, The Netherlands;* orcid.org/0000-0002-2109-9818

A. Mameli − *TNO-Holst Centre, 5656 AE Eindhoven, The Netherlands;* orcid.org/0000-0001-9175-8965

F. Roozeboom − *Department of Applied Physics, Eindhoven University of Technology, 5600 MB Eindhoven, The Netherlands; TNO-Holst Centre, 5656 AE Eindhoven, The Netherlands;* Present Address: University of Twente, Faculty of Science & Technology, P.O. Box 217, 7500 AE Enschede, The Netherlands

Complete contact information is available at: https://pubs.acs.org/10.1021/acs.jpcc.1c07980

Notes

The authors declare no competing financial interest.

■ ACKNOWLEDGMENTS

The authors thank the Material Innovation Institute M2i, the Netherlands Organization for Scientific Research NWO, and the Netherlands Organization for Applied Scientific Research TNO (Holst Centre) for their financial support (NWO-M2i Contract No. F61.4.15561). They also acknowledge the technical assistance provided by F. Grob at the ALD reactor and the RBS/ERD analysis performed by Dr. W. A. Bik.

■ REFERENCES

(1) Gusev, E. P.; Buchanan, D. A.; Cartier, E.; Kumar, A.; DiMaria, D.; Guha, S.; Callegari, A.; Zafar, S.; Jamison, P. C.; Neumayer, D. A. et al. In *Ultrathin High-k Gate Stacks for Advanced CMOS Devices*, Electron Devices Meeting, 2001. IEDM '01. Technical Digest. International, 2001; pp 20.1.1−20.1.4.

(2) Jellison, G. E.; Joshi, P. C. *Crystalline Silicon Solar Cells*; Springer Series in Optical Sciences; Florida Atlantic University: Boca Raton, FL, 2018; Vol. *212*, pp 201−225.

(3) Mayer, A. S.; Kirkpatrick, B. C. Silicon photonics. *Front. Mod. Opt.* **2016**, *24*, 189−205.

(4) Dingemans, G.; van de Sanden, M. C. M.; Kessels, W. M. M. Excellent Si surface passivation by low temperature SiO_2 using an ultrathin Al_2O_3 capping film. *Phys. Status Solidi RRL* **2011**, *5*, 22−24.

(5) Kwon, Y. J.; Jeong, J. K. Recent progress in high performance and reliable n-type transition metal oxide-based thin film transistors. *Semicond. Sci. Technol.* **2015**, *30*, No. 024002.

(6) Howells, D. G.; Henry, B. M.; Madocks, J.; Assender, H. E. High quality plasma enhanced chemical vapour deposited silicon oxide gas barrier coatings on polyester films. *Thin Solid Films* **2008**, *516*, 3081−3088.

(7) Ovanesyan, R. A.; Filatova, E. A.; Elliott, S. D.; Hausmann, D. M.; Smith, D. C.; Agarwal, S. Atomic layer deposition of silicon-based dielectrics for semiconductor manufacturing: current status and future outlook. *J. Vac. Sci. Technol., A* **2019**, *37*, No. 060904.

(8) George, S. M. Atomic layer deposition: an overview. *Chem. Rev.* **2010**, *110*, 111−131.

(9) Knoops, H. C. M.; Faraz, T.; Arts, K.; Kessels, W. M. M. Status and prospects of plasma-assisted atomic layer deposition. *J. Vac. Sci. Technol., A* **2019**, *37*, No. 030902.

(10) Dingemans, G.; van Helvoirt, C. A. A.; Pierreux, D.; Keuning, W.; Kessels, W. M. M. Plasma-assisted ALD for the conformal deposition of SiO_2: process, material and electronic properties. *J. Electrochem. Soc.* **2012**, *159*, H277.

(11) Potts, S. E.; Profijt, H. B.; Roelofs, R.; Kessels, W. M. M. Room-temperature ALD of metal oxide thin films by energy-enhanced ALD. *Chem. Vap. Deposition* **2013**, *19*, 125−133.
(12) Poodt, P.; Cameron, D. C.; Dickey, E.; George, S. M.; Kuznetsov, V.; Parsons, G. N.; Roozeboom, F.; Sundaram, G.; Vermeer, A. Spatial atomic layer deposition: a route towards further industrialization of atomic layer deposition. *J. Vac. Sci. Technol., A* **2012**, *30*, No. 010802.
(13) Muñoz-Rojas, D.; Huong Nguyen, V.; Masse de la Huerta, C.; Jiménez, C.; Bellet, D. Spatial Atomic Layer Deposition. In *Chemical Vapor Deposition for Nanotechnology*; Mandracci, P., Ed.; IntechOpen, 2019.
(14) Poodt, P.; Kniknie, B.; Branca, A.; Winands, H.; Roozeboom, F. Patterned deposition by plasma enhanced spatial atomic layer deposition. *Phys. Status Solidi RRL* **2011**, *5*, 165−167.
(15) Van den Bruele, F. J.; Smets, M.; Illiberi, A.; Creyghton, Y.; Buskens, P.; Roozeboom, F.; Poodt, P. Atmospheric pressure plasma enhanced spatial ALD of silver. *J. Vac. Sci. Technol., A* **2015**, *33*, No. 01A131.
(16) Mione, M. A.; Katsouras, I.; Creyghton, Y.; van Boekel, W.; Maas, J.; Gelinck, G.; Roozeboom, F.; Illiberi, A. Atmospheric pressure plasma enhanced spatial ALD of ZrO_2 for low-temperature, large-area applications. *ECS J. Solid State Sci. Technol.* **2017**, *6*, N243−N249.
(17) Mione, M. A.; Engeln, R.; Vandalon, V.; Kessels, W. M. M.; Roozeboom, F. Infrared and optical emission spectroscopy study of atmospheric pressure plasma-enhanced spatial ALD of Al_2O_3. *Appl. Phys. Lett.* **2019**, *115*, No. 083101.
(18) Hoffmann, L.; Theirich, D.; Pack, S.; Kocak, F.; Schlamm, D.; Hasselmann, T.; Fahl, H.; Raupke, A.; Gargouri, H.; Riedl, T. Gas diffusion barriers prepared by spatial atmospheric pressure plasma enhanced ALD. *ACS Appl. Mater. Interfaces* **2017**, *9*, 4171−4176.
(19) Hoffmann, L.; Theirich, D.; Schlamm, D.; Hasselmann, T.; Pack, S.; Brinkmann, K. O.; Rogalla, D.; Peters, S.; Räupke, A.; Gargouri, H.; et al. Atmospheric pressure plasma enhanced spatial atomic layer deposition of SnO_x as conductive gas diffusion barrier. *J. Vac. Sci. Technol., A* **2018**, *36*, No. 01A112.
(20) Zhang, L.; Xiao, W.; Wu, W.; Liu, B. Research Progress on flexible oxide-based thin film transistors. *Appl. Sci.* **2019**, *9*, No. 773.
(21) Fang, G.; Xu, L.; Ma, J.; Li, A. Theoretical understanding of the reaction mechanism of SiO_2 atomic layer deposition. *Chem. Mater.* **2016**, *28*, 1247−1255.
(22) Miikkulainen, V.; Leskelä, M.; Ritala, M.; Puurunen, R. L. Crystallinity of inorganic films grown by atomic layer deposition: overview and general trends. *J. Appl. Phys.* **2013**, *113*, No. 021301.
(23) Sneh, O.; Wise, M. L.; Ott, A. W.; Okada, L. A.; George, S. M. Atomic layer growth of SiO_2 on Si (100) using $SiCl_4$ and H_2O in a binary reaction sequence. *Surf. Sci.* **1995**, *334*, 135−152.
(24) Klaus, J. W.; George, S. M. Atomic Layer Deposition of SiO_2 at Room temperature using NH_3-catalyzed sequential surface reactions. *Surf. Sci.* **2000**, *447*, 81−90.
(25) Murray, C. A.; Elliott, S. D.; Hausmann, D.; Henri, J.; Lavoie, A. Effect of reaction mechanism on precursor exposure time in atomic layer deposition of silicon oxide and silicon nitride. *ACS Appl. Mater. Interfaces* **2014**, *6*, 10534−10541.
(26) Jeong, Y. C.; Baek, S. B.; Kim, D. H.; Kim, J. S.; Kim, Y. C. Initial reaction of silicon precursors with a varying number of dimethylamino ligands on a hydroxyl-terminated silicon (001) surface. *Appl. Surf. Sci.* **2013**, *280*, 207−211.
(27) Lim, J. W.; Yun, S. J.; Lee, J. H. Low-temperature growth of SiO_2 films by plasma-enhanced atomic layer deposition. *ETRI J.* **2005**, *27*, 118−121.
(28) Kinoshita, Y.; Hirose, F.; Miya, H.; Hirahara, K.; Kimura, Y.; Niwano, M. Infrared study of tris(dimethylamino)silane adsorption and ozone irradiation on Si (100) surfaces for ALD of SiO_2. *Electrochem. Solid-State Lett.* **2007**, *10*, G80−G83.
(29) Hirose, F.; Kinoshita, Y.; Shibuya, S.; Miya, H.; Hirahara, K.; Kimura, Y.; Niwano, M. Atomic-Layer-Deposition of SiO_2 with tris(dimethylamino)silane (TDMAS) and ozone investigated by infrared absorption spectroscopy. *ECS Trans.* **2008**, *13*, 171−177.
(30) Potts, S. E.; Profijt, H. B.; Roelofs, R.; Kessels, W. M. M. Room-temperature ald of metal oxide thin films by energy-enhanced ALD. *Chem. Vap. Deposition* **2013**, *19*, 125−133.
(31) Peña, L. F.; Nanayakkara, C. E.; Mallikarjunan, A.; Chandra, H.; Xiao, M.; Lei, X.; Pearlstein, R. M.; Derecskei-Kovacs, A.; Chabal, Y. J. Atomic layer deposition of silicon dioxide using aminosilanes di-sec-butylaminosilane and bis(tert-butylamino)silane with ozone. *J. Phys. Chem. C* **2016**, *120*, 10927−10935.
(32) Lu, Y.; Kobayashi, A.; Kondo, H.; Ishikawa, K.; Sekine, M.; Hori, M. Chemical reactions during plasma-enhanced atomic layer deposition of SiO_2 films employing aminosilane and O_2/Ar plasma at 50 °C. *Jpn. J. Appl. Phys.* **2014**, *53*, No. 010305.
(33) Putkonen, M.; Bosund, M.; Ylivaara, O. M. E.; Puurunen, R. L.; Kilpi, L.; Ronkainen, H.; Sintonen, S.; Ali, S.; Lipsanen, H.; Liu, X.; Haimi, E.; Hannula, S. P.; Sajavaara, T.; et al. Thermal and plasma enhanced atomic layer deposition of SiO_2 using commercial silicon precursors. *Thin Solid Films* **2014**, *558*, 93−98.
(34) Huang, L.; Han, B.; Derecskei-Kovacs, A.; Xiao, M.; Lei, X.; O'Neill, M. L.; Pearlstein, R. M.; Chandra, H.; Cheng, H. First-principles study of a full cycle of atomic layer deposition of SiO_2 thin films with di(sec-butylamino)silane and ozone. *J. Phys. Chem. C* **2013**, *117*, 19454−19463.
(35) Peña, L. F.; Mattson, E. C.; Nanayakkara, C. E.; Oyekan, K. A.; Mallikarjunan, A.; Chandra, H.; Xiao, M.; Lei, X.; Pearlstein, R. M.; Derecskei-Kovacs, A.; et al. In situ infrared absorption study of plasma-enhanced atomic layer deposition of silicon nitride. *Langmuir* **2018**, *34*, 2619−2629.
(36) Huang, L.; Han, B.; Fan, M.; Cheng, H. Design of efficient mono-aminosilane precursors for atomic layer deposition of SiO_2 thin films. *RSC Adv.* **2017**, *7*, 22672−22678.
(37) Mallikarjunan, A.; Chandra, H.; Xiao, M.; Lei, X.; Pearlstein, R. M.; Bowen, H. R.; O'Neill, M. L.; Derecskei-Kovacs, A.; Han, B. Designing high performance precursors for atomic layer deposition of silicon oxide. *J. Vac. Sci. Technol., A* **2015**, *33*, No. 01A137.
(38) Kamiyama, S. N.; Miura, T.; Nara, Y. Comparison between SiO_2 films deposited by atomic layer deposition. *Thin Solid Films* **2006**, *515*, 1517−1521.
(39) Han, B.; Zhang, Q.; Wu, J.; Han, B.; Karwacki, E. J.; Derecskei, A.; Xiao, M.; Lei, X.; O'Neill, M. L.; Cheng, H. On the mechanisms of SiO_2 thin-film growth by the full atomic layer deposition process using bis(t-butylamino)silane on the hydroxylated SiO_2 (001) surface. *J. Phys. Chem. C* **2012**, *116*, 947−952.
(40) O'Neill, M. L.; Bowen, H. R.; Derecskei-Kovacs, A.; Cuthill, K. S.; Han, B.; Xiao, M. Silicon oxides by atomic layer deposition. *Electrochem. Soc. Interface* **2011**, *20*, 33−37.
(41) Baek, S. B.; Kim, D. H.; Kim, Y. C. Adsorption and surface reaction of bis-diethylaminosilane as a Si precursor on an OH-terminated Si (001) surface. *Appl. Surf. Sci.* **2012**, *258*, 6341−6344.
(42) Burton, B. B.; Rang, S. W.; Rhee, S. W.; George, S. M. SiO_2 Atomic layer deposition using tris(dimethylamino)silane and hydrogen peroxide studied by in situ transmission FTIR spectroscopy. *J. Phys. Chem. C* **2009**, *113*, 8249−8257.
(43) Fang, G. Y.; Xu, L. N.; Cao, Y. Q.; Wang, L. G.; Wu, D.; Li, A. D. Self-catalysis by aminosilanes and strong surface oxidation by O_2 plasma in plasma-enhanced atomic layer deposition of high-quality SiO_2. *Chem. Commun.* **2015**, *51*, 1341−1344.
(44) Li, J.; Wu, J.; Wu, C. Z.; Han, B.; Karwacki, E. J.; Xiao, M.; Lei, X.; Cheng, H. On the dissociative chemisorption of tris-(dimethylamino)silane on hydroxylated SiO_2(001) surface. *J. Phys. Chem. C* **2009**, *113*, 9731−9736.
(45) Suzuki, I.; Yanagita, K.; Dussarrat, C. Extra low-temperature SiO_2 deposition using aminosilanes. *ECS Trans.* **2019**, *3*, 119−128.
(46) Kobayashi, A.; Tsuji, N.; Fukazawa, A.; Kobayashi, N. Temperature dependence of SiO_2 film growth with plasma-enhanced atomic layer deposition. *Thin Solid Films* **2012**, *520*, 3994−3998.
(47) Won, S. J.; Suh, S.; Huh, M. S.; Kim, H. J. High-Quality Low-temperature silicon oxide by plasma-enhanced atomic layer deposition

using a metalorganic silicon precursor and oxygen radical. *IEEE Electron Device Lett.* **2010**, *31*, 857−859.
(48) Leick, N.; Huijs, J. M. M.; Ovanesyan, R. A.; Hausmann, D. M.; Agarwal, S. Surface reactions of aminosilane precursors during N_2 plasma-assisted atomic layer deposition of SiN_x. *Plasma Processes Polym.* **2019**, *16*, No. 1900032.
(49) Potts, S. E.; Keuning, W.; Langereis, E.; Dingemans, G.; van de Sanden, M. C. M.; Kessels, W. M. M. Low temperature plasma-enhanced atomic layer deposition of metal oxide thin films. *J. Electrochem. Soc.* **2010**, *157*, P66.
(50) Poodt, P.; Lankhorst, A.; Roozeboom, F.; Spee, K.; Maas, D.; Vermeer, A. High-speed spatial atomic-layer deposition of aluminum oxide layers for solar cell passivation. *Adv. Mater.* **2010**, *22*, 3564−3567.
(51) Muñoz-Rojas, D.; Maindron, T.; Esteve, A.; Piallat, F.; Kools, J. C. S.; Decams, J. M. Speeding up the unique assets of atomic layer deposition. *Mater. Today Chem.* **2019**, *12*, 96−120.
(52) Creyghton, Y.; Illiberi, A.; Mione, M. A.; van Boekel, W.; Debernardi, N.; Seitz, M.; van den Bruele, F.; Poodt, P.; Roozeboom, F. Plasma-enhanced atmospheric-pressure spatial ALD of Al_2O_3 and ZrO_2. *ECS Trans.* **2016**, *75*, 11−19.
(53) Zhuravlev, L. T. The Surface chemistry of amorphous silica. *Colloids Surf., A* **2000**, *173*, 1−38.
(54) Langereis, E.; Keijmel, J.; van de Sanden, M. C. M.; Kessels, W. M. M. Surface chemistry of plasma-assisted atomic layer deposition of Al_2O_3 studied by infrared spectroscopy. *Appl. Phys. Lett.* **2008**, *92*, No. 231904.
(55) Bosch, R. H. E. C.; Cornelissen, L. E.; Knoops, H. C. M.; Kessels, W. M. M. Atomic layer deposition of silicon nitride from bis(tertiary-butyl-amino)silane and N_2 plasma studied by in situ gas phase and surface infrared spectroscopy. *Chem. Mater.* **2016**, *28*, 5864−5871.
(56) Newhouse, E. I. Computations of Vibrational Infrared Frequencies of Selected Amines. Ph.D. Thesis, Pennsylvania University, Philadelphia, 1990.
(57) Katamreddy, R.; Feist, B.; Takoudis, C. Bis(Diethylamino) Silane as the Silicon Precursor in the Atomic Layer Deposition of $HfSiO_x$. *J. Electrochem. Soc.* **2008**, *155*, G163.
(58) Giovannetti, R.; Alibabaei, L.; Samanipour, S. Structure investigations of binary azeotrope of diethyl amine-acetone by FT-IR and (1)H NMR Spectroscopy. *Spectrochim. Acta, Part A* **2009**, *72*, 390−393.
(59) Rai, V. R.; Vandalon, V.; Agarwal, S. Surface reaction mechanisms during ozone and oxygen plasma assisted atomic layer deposition of aluminum oxide. *Langmuir* **2010**, *26*, 13732−13735.
(60) Rai, V. R.; Agarwal, S. Surface reaction mechanisms during plasma-assisted atomic layer deposition of titanium dioxide. *J. Phys. Chem. C* **2009**, *113*, 12962−12965.
(61) Eliasson, B.; Hirth, M.; Kogelschatz, U. Ozone synthesis from oxygen in dielectric barrier discharges. *J. Phys. D: Appl. Phys.* **1987**, *20*, 1421−1437.
(62) Schmidt-Bleker, A.; Winter, J.; Bösel, A.; Reuter, S.; Weltmann, K. D. On the plasma chemistry of a cold atmospheric Argon plasma jet with shielding gas device. *Plasma Sources Sci. Technol.* **2015**, *25*, No. 015005.
(63) Liu, Y.; Welzel, S.; Starostin, S. A.; van de Sanden, M. C. M.; Engeln, R.; de Vries, H. W. Infrared gas phase study on plasma-polymer interaction in high-current dielectric barrier discharges. *J. Appl. Phys.* **2017**, *121*, No. 243301.
(64) Heil, S. B. S.; Roozeboom, F.; van de Sanden, M. C. M.; Kessels, W. M. M. Plasma-assisted atomic layer deposition of Ta_2O_5 from alkylamide precursor and remote O_2 plasma. *J. Vac. Sci. Technol., A* **2008**, *26*, 472−480.
(65) Heil, S. B. S.; van Hemmen, J. L.; van de Sanden, M. C. M.; Kessels, W. M. M. Reaction mechanisms during plasma-assisted atomic layer deposition of metal oxides: a case study for Al_2O_3. *J. Appl. Phys.* **2008**, *103*, No. 103302.
(66) Pokrovski, K.; Jung, K. T.; Bell, A. T. Investigation of CO and CO_2 Adsorption on tetragonal and monoclinic zirconia. *Langmuir* **2001**, *17*, 4297−4303.
(67) Heil, S. B. S.; Kudlacek, P.; Langereis, E.; Engeln, R.; van de Sanden, M. C. M.; Kessels, W. M. M. In situ reaction mechanism studies of plasma-assisted atomic layer deposition of Al_2O_3. *Appl. Phys. Lett.* **2006**, *89*, No. 131505.

https://doi.org/10.1021/acs.jpcc.1c07980
J. Phys. Chem. C 2021, 125, 24945−24957